LBL-34471
UC-331
Preprint

Lawrence Berkeley Laboratory
UNIVERSITY OF CALIFORNIA

Materials Sciences Division

Submitted to Journal of the Electrochemical Society

Relaxation Phenomena in Lithium Ion Insertion Cells

T.F. Fuller, M. Doyle, and J. Newman

October 1993

Prepared for the U.S. Department of Energy under Contract Number DE-AC03-76SF00098

DISCLAIMER

LBL-34471
UC-331

Relaxation Phenomena in Lithium Ion Insertion Cells

Thomas F. Fuller, Marc Doyle, and John Newman

Department of Chemical Engineering
University of California

and

Materials Sciences Division
Lawrence Berkeley Laboratory
University of California
Berkeley, California 94720

October 1993

This work was supported in part by the Assistant Secretary for Energy Efficiency and Renewable Energy, Office of Transportation Technologies, Electric and Hybrid Propulsion Division of the U. S. Department of Energy under Contract No. DE-AC03-76SF00098.

Relaxation Phenomena in Lithium Ion Insertion Cells

Thomas F. Fuller, Marc Doyle, and John Newman

Department of Chemical Engineering
University of California
and
Materials Sciences Division
Lawrence Berkeley Laboratory
University of California
Berkeley, California 94720

Abstract

Relaxation phenomena in lithium-ion-insertion cells are modeled. Simulation results are presented for a dual lithium-ion-insertion cell and for a cell using a lithium-foil negative electrode. A period of relaxation after a charge or discharge can cause appreciable changes in the distribution of material in the insertion electrodes. Local concentration cells in the solution phase and an open-circuit potential that depends on state of charge for the solid phase drive the redistribution of material. Concentration profiles in solid and solution phases during relaxation are analyzed, and the consequences for cell performance are discussed. The model predicts the effects of relaxation time on multiple charge-discharge cycles and on peak power. Galvanostatic and potentiostatic charging are simulated; the results are compared to experimental data for a commercial battery.

Introduction

The mathematical model of the lithium-ion-insertion cell of Doyle *et al.*[1,2] can be used to study the effects of relaxation times on the performance of these systems. Both in laboratory work and in practical usage, it is expected that there will be significant times during which cells are allowed to stand without passing current through an external circuit. The cell is not inactive during these periods; rather, concentration gradients in the cell set up

local concentration cells, driving material redistribution. Because high utilization of active material is important for maximizing the specific energy, understanding the redistribution of material is a necessary step in the optimization of lithium-ion cells. Also, because of the changes that take place during relaxation, the number of completed cycles, *i.e.*, the history of the cell, can affect its performance (irreversible degradation processes are not considered). A detailed mathematical model can predict aspects of cell performance, such as material utilization, that are difficult to assess by experimental means. Modeling is also important in the design and scale-up of practical systems.

Because of the high theoretical specific energy, lithium rechargeable cells are being targeted for electric-vehicle applications as well as portable appliances. Interest in lithium-ion cells has surged since Sony[3] commercialized a dual lithium-ion-insertion battery with a specific energy of about 80 Wh/kg. We will consider two different systems in our study of relaxation processes; both types are receiving much attention in the literature. The first cell consists of a lithium-foil negative electrode coupled with a manganese dioxide (spinel) positive electrode. The second cell is the Sony phone cell, which uses two different insertion electrodes with differing open-circuit potentials (a "rocking-chair" cell).

We will not repeat the details of the model of Doyle *et al.* The pertinent equations are summarized in appendix A; more information can be found in references 1 and 2. The model uses concentrated solution theory with variable transport properties to describe transport in the electrolyte. Insertion electrodes are treated with porous electrode theory, assuming a constant diffusion coefficient in the solid phase. Film formation at the electrode surfaces and volume changes are neglected in the present model. Pollard and Newman[4] have done a similar analysis of relaxation phenomena for the lithium-aluminum iron sulfide system.

Results and Discussion

Model parameters and systems analyzed.—The two cells studied are depicted in figure 1. The first is a lithium foil/polymer electrolyte/insertion material cell; the second is a

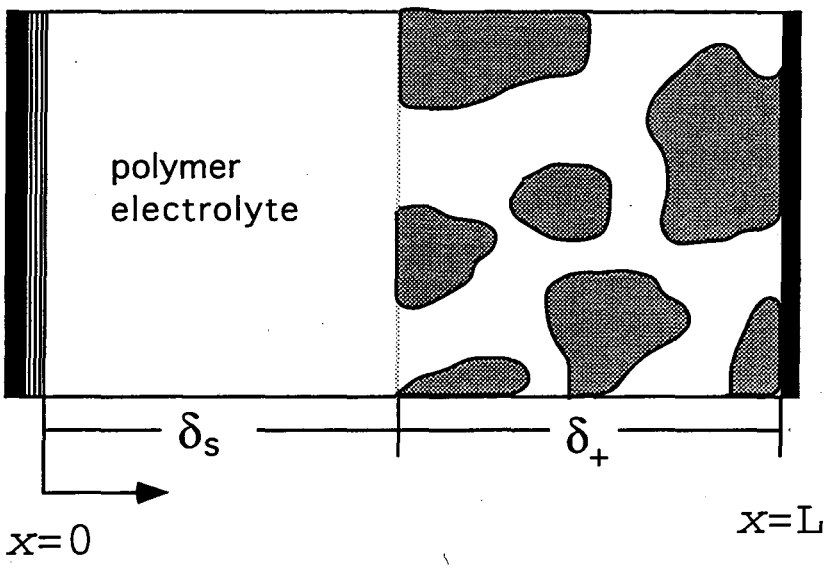

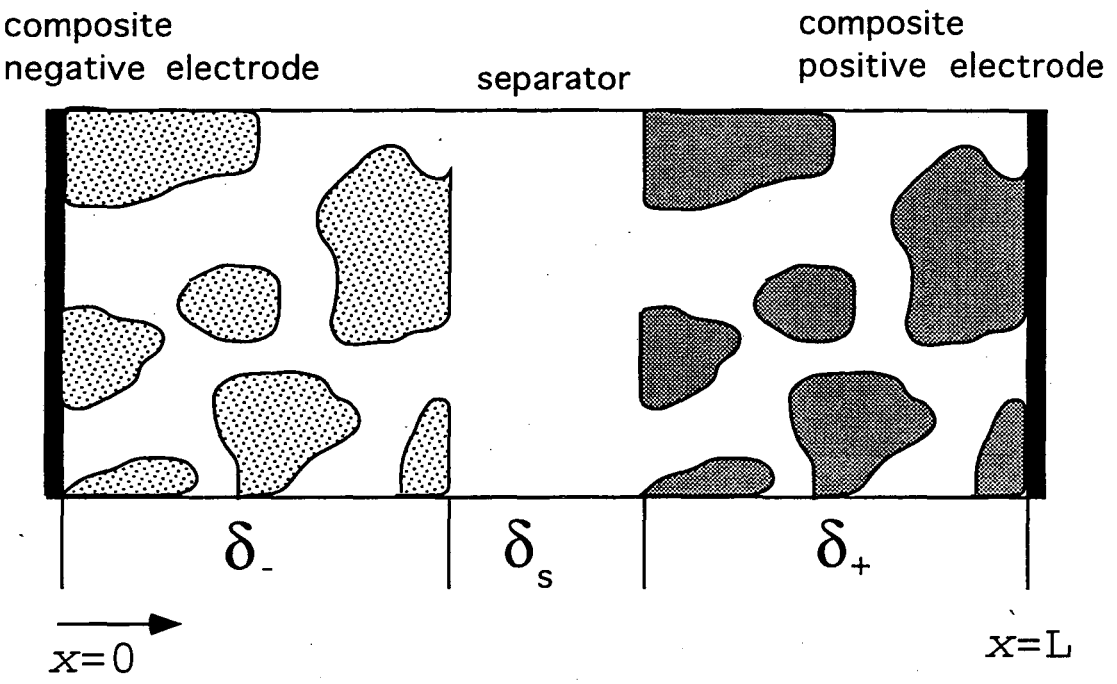

Figure 1. Lithium insertion cells. Upper cell contains a lithium foil negative electrode. The lower cell ("rocking-chair" type) has a carbon negative electrode.

dual lithium-ion-insertion system. For the foil cell, the positive electrode is manganese dioxide, the negative electrode is lithium, and the electrolyte is a solid polymer electrolyte (polyethylene oxide with lithium trifluormethane sulfonate. For the dual insertion system, the positive electrode is cobalt dioxide), the negative electrode is carbon, and the electrolyte is a nonaqueous liquid (propylene carbonate/diethyl carbonate with lithium hexafluorophosphate). Each insertion electrode is a porous composite structure containing the active insertion material, filler of inert conducting material and/or binder, and electrolyte. We have assumed that the electrical conductivity of the solid phase is moderately large and that the kinetic resistances to the insertion process are small. Transport properties for the electrolytes are listed in appendix B. The parameters for the two electrodes are given in tables 1 and 2. The open-circuit potentials for the electrodes are given in appendix B.

Table 1.

Parameters used in the lithium-foil simulations.

System specific			Design adjustable	
Parameter	Value	Reference	Parameter	Value
D_s	10^{-13} m^2/s	5	T	80°C
σ	100 S/m	†	δ_s	50 μm
$i_{o,1}$	12.6 A/m^2	6,*	δ_+	100 μm
c_t	23,720 mol/m^3	‡	ε	0.4
ν_+,ν_-	1	-	ε_f	0.1
α_a,α_c	0.5	†	c^o	1500 mol/m^3
$i_{o,2}$	13.1	†	R_s	2 μm

* Value reported at initial conditions

† Assumed values.

‡ Calculated based on the density of the insertion material with y or x equal to one.

Table 2.

Parameters for the electrodes of dual-ion-insertion cell.

Parameter	Li_xC_6	Ref.	Li_yCoO_2	Ref.
D_s (m^2/s)	5×10^{-13}	5	5×10^{-13}	7
σ (S/m)	100	†	100	†
α_c,α_a	0.5	†	0.5	†
c_t (mol/m^3)	24,190	‡	54,630	‡
i_o (A/m^2)	2.15	†	4.89	8*

Design adjustable parameters for dual ion-insertion cell.

Parameter	Li_xC_6	Li_yCoO_2
δ_-, δ_+ (μm)	252	165
R_s (μm)	4	4
c_s^o (mol/m^3)	14,089	30,938
ε	0.44	0.36
ε_f	0.0795	0.05815

Parameter	Value
T	25°C
c^o	1400 mol/m^3
ε_s	0.38
δ_s	25 μm
z	1.791

* Value reported at initial conditions

† Assumed values.

‡ Calculated based on the density of the insertion material with y or x equal to one.

Relaxation phenomena.—There are several phenomena associated with the relaxation of the cells, typically with widely varying time constants. When the external current is interrupted, for example, we can identify three transients: relaxation of the double-layer capacitance, local equalization of the state of charge, and reduction of concentration gradients in the solid insertion material and in the electrolyte. The model does not include a double-layer capacitance; hence double-layer charging and discharging, expected to occur on the ms time scale ($\tau = L^2 aC/\kappa$),[9] are not represented here. For transport in the electrolyte and transport in the solid insertion materials, the time constants can be compared to the time of discharge.[2] In the positive electrode, for example,

$$S_s = \frac{R_s^2 I}{D_s nF(1-\varepsilon-\varepsilon_f)(c_t - c_s^o)\delta_+} . \qquad (1)$$

S_s is the ratio of diffusion time to discharge time. This dimensionless ratio allows one to assess the importance of diffusion in the solid matrix relative to the time for discharge. For $S_s << 1$, diffusion limitations in the particle can be neglected.

We can also develop a ratio of the time constant for diffusion in the electrolyte and the time of discharge,

$$S_e = \frac{L^2 I}{DnF(1-\varepsilon-\varepsilon_f)(c_t - c_s^o)\delta_+} . \qquad (2)$$

This ratio indicates whether sufficient time is available for a quasi-steady-state concentration gradient to be established over the course of the discharge or charge.

Lithium-foil cell.—Figure 2 shows the cell potential over one discharge/charge cycle. Manganese dioxide has been demonstrated to insert lithium over a wide range of compositions, corresponding to $0.2<y<2.4$ in $Li_yMn_2O_4$.[5,11] We have chosen to use only

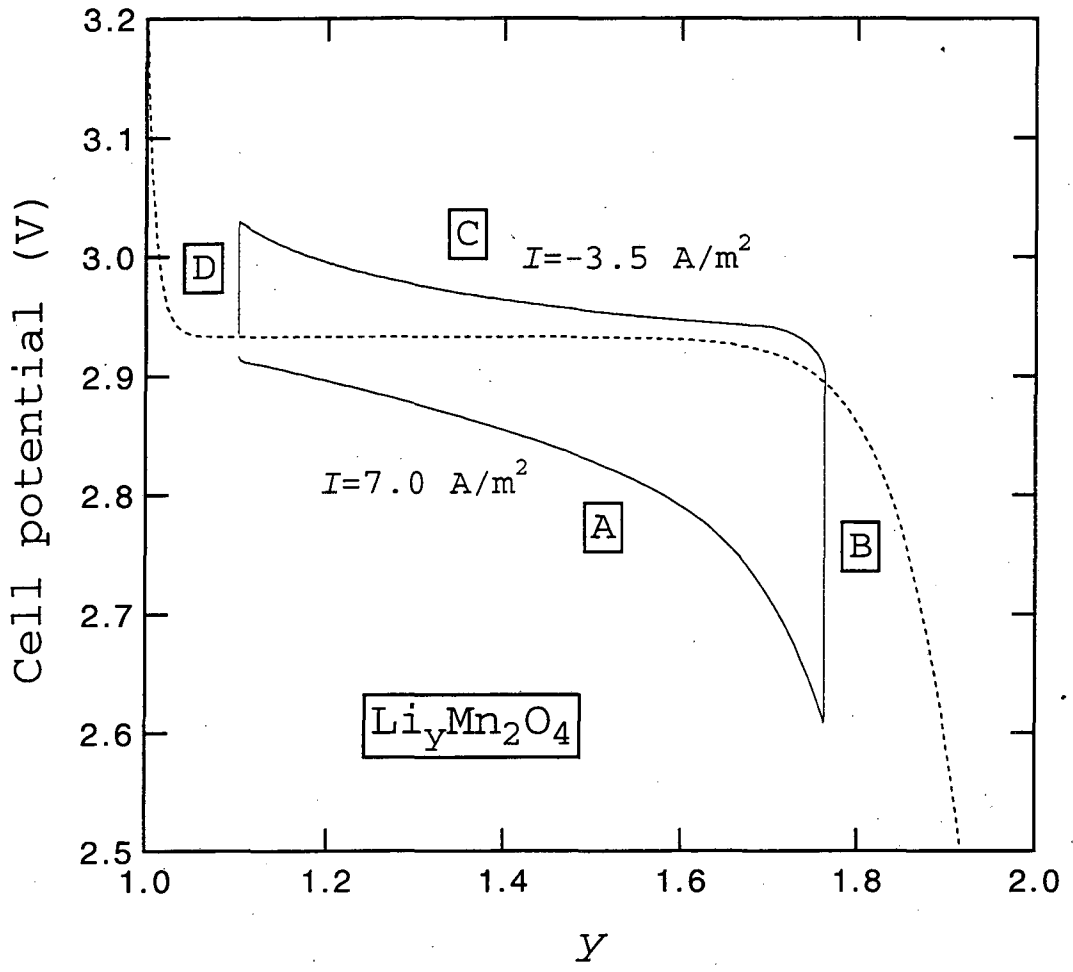

Figure 2. Cell potential *vs.* state of charge for the lithium/manganese dioxide system during a complete discharge/charge cycle at I=7.0 A/m^2 and I=-3.5 A/m^2, respectively. The cell is allowed to relax for one hour between each half cycle (B and D). The dashed line is the open-circuit potential of the cell.

the lower plateau region in this simulation, corresponding to about $1.1<y<1.8$. The trade-offs involved in selecting a composition range over which to cycle a cell have been discussed previously for this system and for the lithium-iron disulfide system,[10] where a similar situation exists. The dashed line indicates the open-circuit potential of the cell, obtained from data of Macklin *et al.*[11]

The cell is discharged galvanostatically at the three-hour rate (7.0 A/m^2). The discharge is labeled section A in figure 2. When $y \approx 1.76$, the external current is interrupted, and the cell is allowed to relax for one hour; this is labeled section B. Following a small ohmic jump, the cell potential relaxes and approaches the open-circuit value. The change in potential is the result of relaxation of concentration gradients in the electrolyte and in the solid particles. There is also a redistribution of lithium in the solid matrix. With the cell current at zero ($I = 0$), lithium deinserts from the front of the positive electrode and inserts in the back of the electrode. The redistribution of lithium occurs without changing the net state of charge of the electrode. Next, the cell is charged galvanostatically at -3.50 A/m^2 (six-hour rate) to the original state of charge, labeled as section C. The current is interrupted, and again the cell is allowed to relax for one hour (labeled D).

The behavior of the system during discharge, section A of figure 2, has been the object of previous study and thus will not be given a detailed examination here.[1] We will merely summarize some general aspects of the behavior of these systems on discharge that are important for the present purposes. First, large concentration gradients in the electrolyte develop because of the small transference number for the lithium ion. A calculation of the dimensionless ratio for transport in solution discussed above gives $S_e \approx 0.2$, suggesting that the concentration profile is established relatively quickly in comparison to the time for discharge. Toward the end of discharge at $I = 7.0$ A/m^2, the concentration is nearly zero in the back of the porous electrode, making the active material in the back of the electrode increasingly difficult to access. The reaction rate distribution

during discharge is nonuniform. The nonuniformity is caused by the large exchange-current density for the insertion process, low solution conductivity, and the flat $U(c_s)$ curve in this region. The insertion reaction moves through the electrode like a spike, consuming most of the available active material before proceeding further. The solid phase is assumed to be composed of spherical particles with an average radius of two microns. For this system, transport in the solid phase is facile. Even with the relatively small diffusion coefficient of lithium in the solid phase, the particles are small enough and the discharge rate low enough that the concentration inside the particles is nearly uniform.

Figure 3 shows the relaxation of the concentration gradients in the cell, corresponding to section B of figure 2. Time from the point of current interruption is given in as a parameter. The concentration gradients relax in about one hour for this system, in qualitative agreement with the value of $S_e \approx 0.2$ found above. One may notice that the concentration profiles do not represent free diffusion; there exists a significant driving force for the redistribution of active material in the solid phase. The front of the electrode is at a lower open-circuit potential than the back of the electrode because these regions are left at differing states of charge after the incomplete discharge. This difference forces lithium to deinsert from the front region and insert into the back of the electrode. The concentration gradients in the electrolyte provide an additional driving force for lithium redistribution. In opposition to the local state of charge, concentration gradients in the electrolyte drive insertion in regions of high electrolyte concentration and deinsertion in regions of low concentration. In the present case, the former phenomenon is dominant, as can be inferred from the curvature of the concentration profiles. Both of these processes occur without changing the net state of charge of the electrode.

During relaxation of the cell, the amount of lithium inserted and deinserted must be equal. In figure 4, we show the pore-wall flux, directly related to the transfer-current density, in the back half of the positive electrode. This back region of the electrode, where active material was not utilized during discharge, is quickly filled during relaxation. The

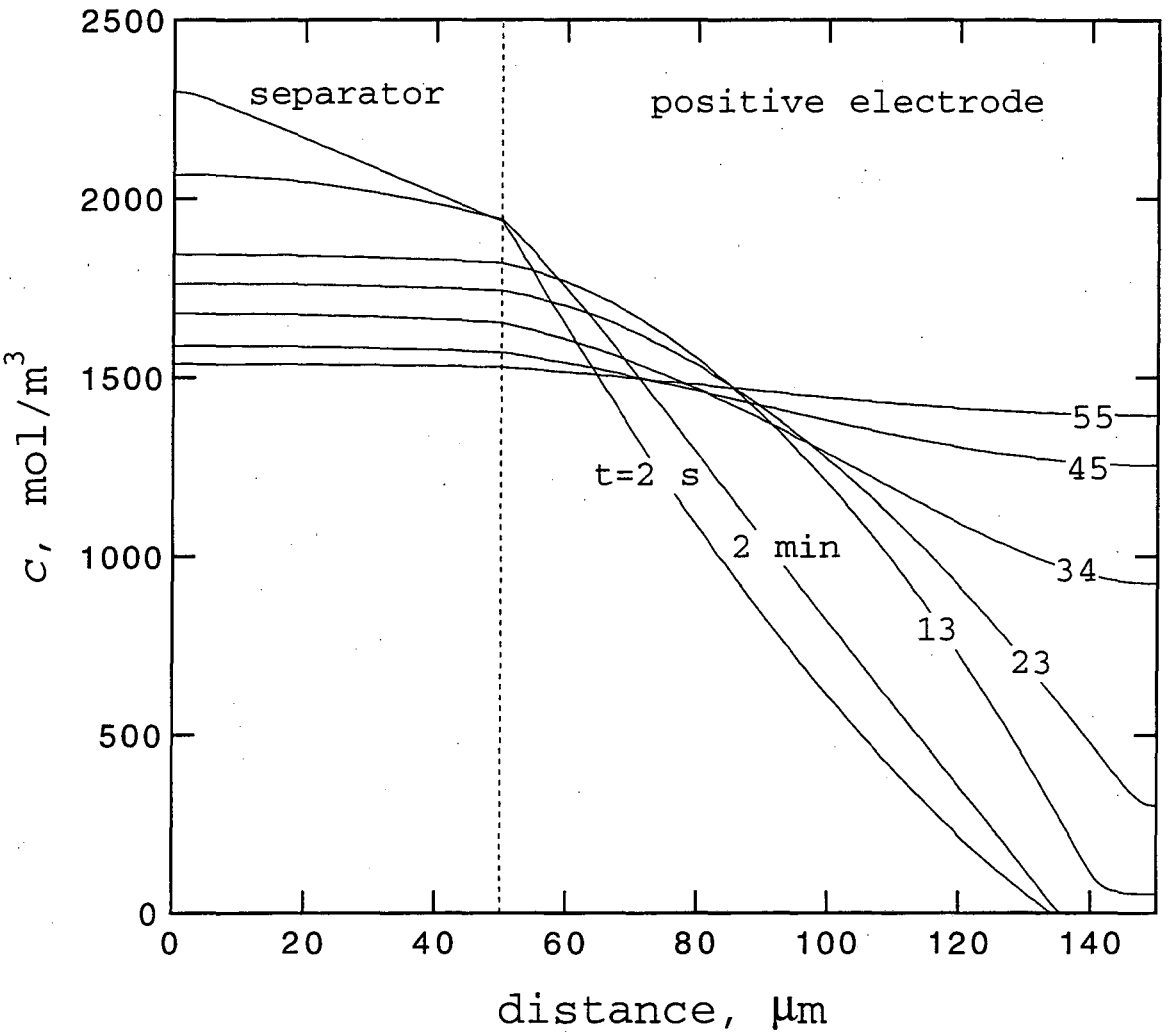

Figure 3. Solution-phase concentration across the cell after the interruption of current. The curves correspond to section B on figure 2. Time since the end of discharge is given as a parameter. The separator/positive electrode boundary is denoted by the dashed line.

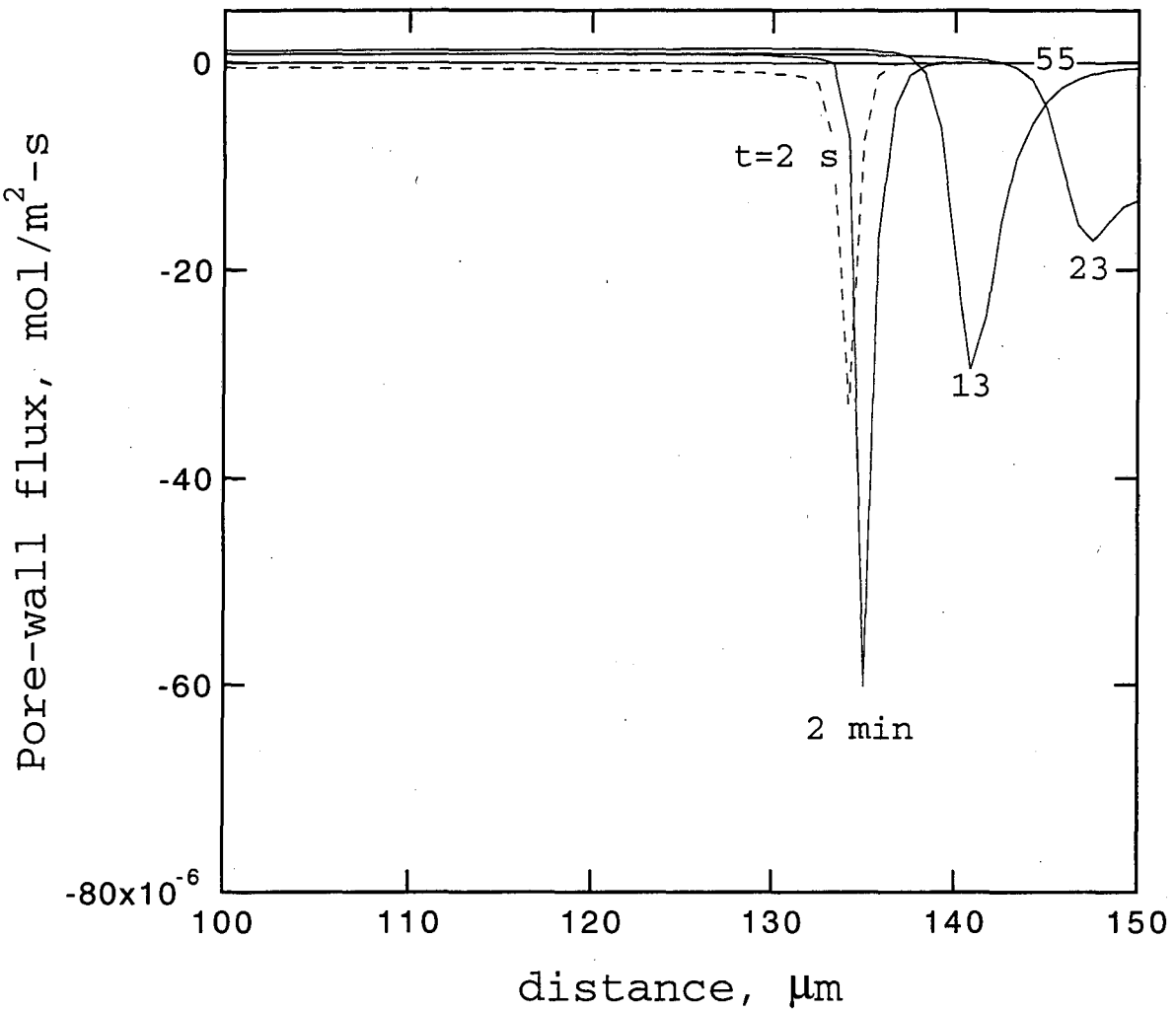

Figure 4. Pore-wall flux into the solid phase across the back half of the positive electrode during relaxation after a discharge at I=7.0 A/m^2. The curves correspond to section B on figure 2. Time since the end of the discharge is given as a parameter. Distance is measured from the negative electrode/separator interface.

reaction distribution resembles a spike during this process, similar to the reaction distribution during discharge. However, along with the insertion in the back region, there is also an equal amount of lithium deinsertion from the front region (shown only partly in figure 4). The deinsertion process occurs uniformly from the front of the electrode since the open-circuit potential is a strong function of state of charge in this region.

Another way of examining the redistribution of lithium is presented in figure 5, which gives the concentration of lithium in the solid particles across the back half of the positive electrode. The concentration in the solid particles is expressed in terms of the parameter y in $Li_yMn_2O_4$, here taken to be the local state of charge of the electrode. The parameter y in $Li_yMn_2O_4$ corresponds to the solid concentration divided by c_t. We show the state of charge at the surface, which in this case is equal to the interior state of charge because diffusion in the particles is fast. Examining figure 5, we see that after 45 minutes of relaxation the state of charge of the electrode has gone from a nonuniform "step" function to a completely uniform distribution of active material. This will have implications for the subsequent charge.

Next, the cell is charged galvanostatically at -3.50 A/m^2 to the initial state of charge, labeled as section C on figure 2. The six-hour rate chosen here is half that used for the discharge. Figure 6 depicts the concentration profiles in the electrolyte during the charging process, for specified times since the beginning of charge. As before, the concentration gradients are established fairly quickly in comparison to the charging time, and a quasi-steady-state profile exists. This profile is slowly modified by the deinsertion process, which again continues as a reaction spike traveling from the front to the back of the positive electrode. At the end of charge, the maximum concentration attained in the cell is about 2480 mol/m^3. Since the solubility limit for this system is assumed to be 3920 mol/m^3,[12] precipitation of salt does not occur at this charging rate. This suggests that a higher initial concentration might have been better for this cell, as this would eliminate the electrolyte depletion problems on discharge.[1] The initial concentration used here

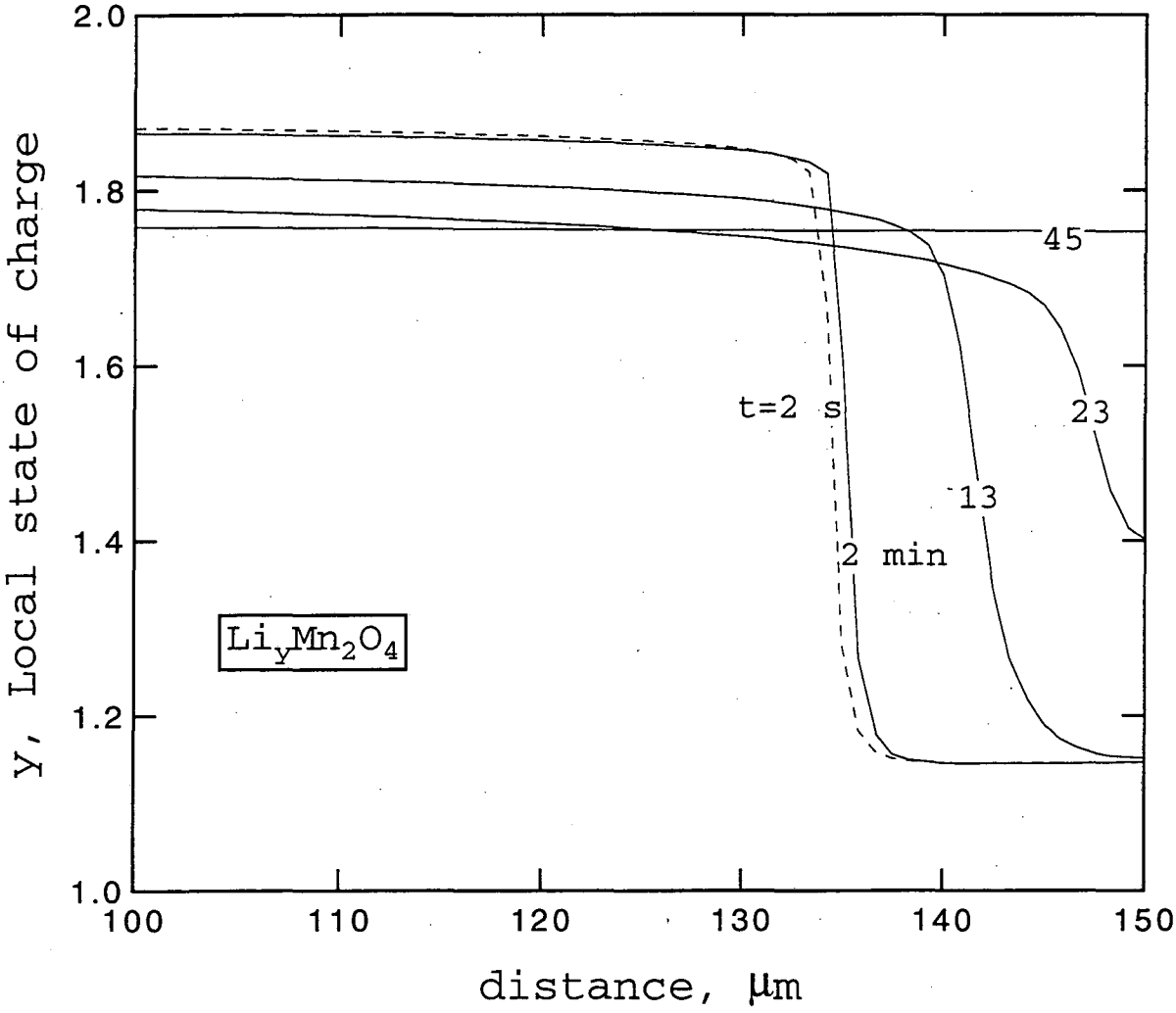

Figure 5. Local state of charge across the back half of the positive electrode during relaxation after a discharge at I=7.0 A/m^2. The curves correspond to section B on figure 2. Time since the end of discharge is given as a parameter. Distance is measured from the negative electrode/separator interface.

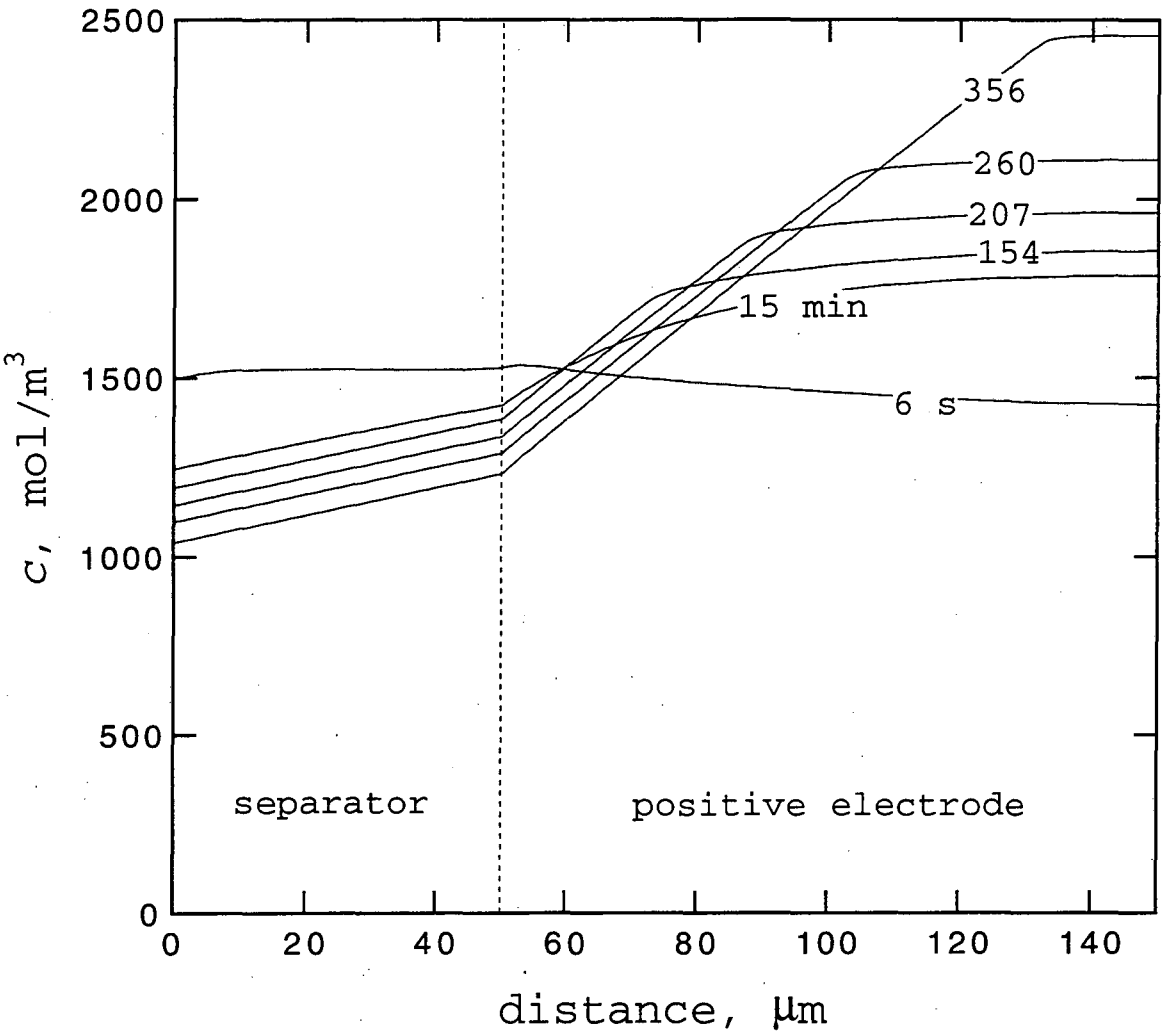

Figure 6. Solution-phase concentration across the cell during charge at I=-3.50 A/m^2. The curves correspond to section C on figure 2. Time since the beginning of the charge is given as a parameter. The separator/positive electrode boundary is denoted by a dashed line.

corresponds to a conductivity maximum for this temperature,[12] roughly equating to $PEO_{18}LiCF_3SO_3$.

The local state of charge across the positive electrode during the charging process is shown in figure 7. Just as in figure 5, this graph provides the concentration of lithium at the surface of the solid particles. The initially uniform distribution across the electrode (due to the relaxation time prior to charge) is perturbed greatly as the reaction zone moves through the electrode. At the end of the charge, we find a region in the back of the electrode where the active material is still utilized, similar to the unutilized region left in the back of the electrode after discharge.

When the cell is allowed to relax for another one-hour period (section D on figure 2), we find a different result from that of figure 5. Figure 8 gives the state of charge across the back half of the positive electrode during this relaxation period. Some lithium deinserts from the back face and inserts into the front region, but in contrast to the relaxation period following discharge, the local state of charge does not fully equalize. We can explain this on the basis of the driving forces for redistribution that were discussed earlier. First, examining the open-circuit potential of manganese dioxide in the region of interest (the dashed line in figure 2), we see that at the end of the charging process the electrode is at a uniform potential. This is in contrast to the situation after discharge, which left the front face at a much reduced potential compared to the back face. Therefore, there is little solid-phase driving force for redistribution of material. The driving force for the solution-phase concentration cell, which causes material to insert at regions of high concentration and to deinsert from regions of low concentration, is weak. Furthermore, this mode of equalization is inherently limited since the concentration profile is simultaneously relaxing due to the diffusion process, and variations in the local utilization dominate the equilization process. Consequently, lithium deinserts from the back of the positive electrode during relaxation.

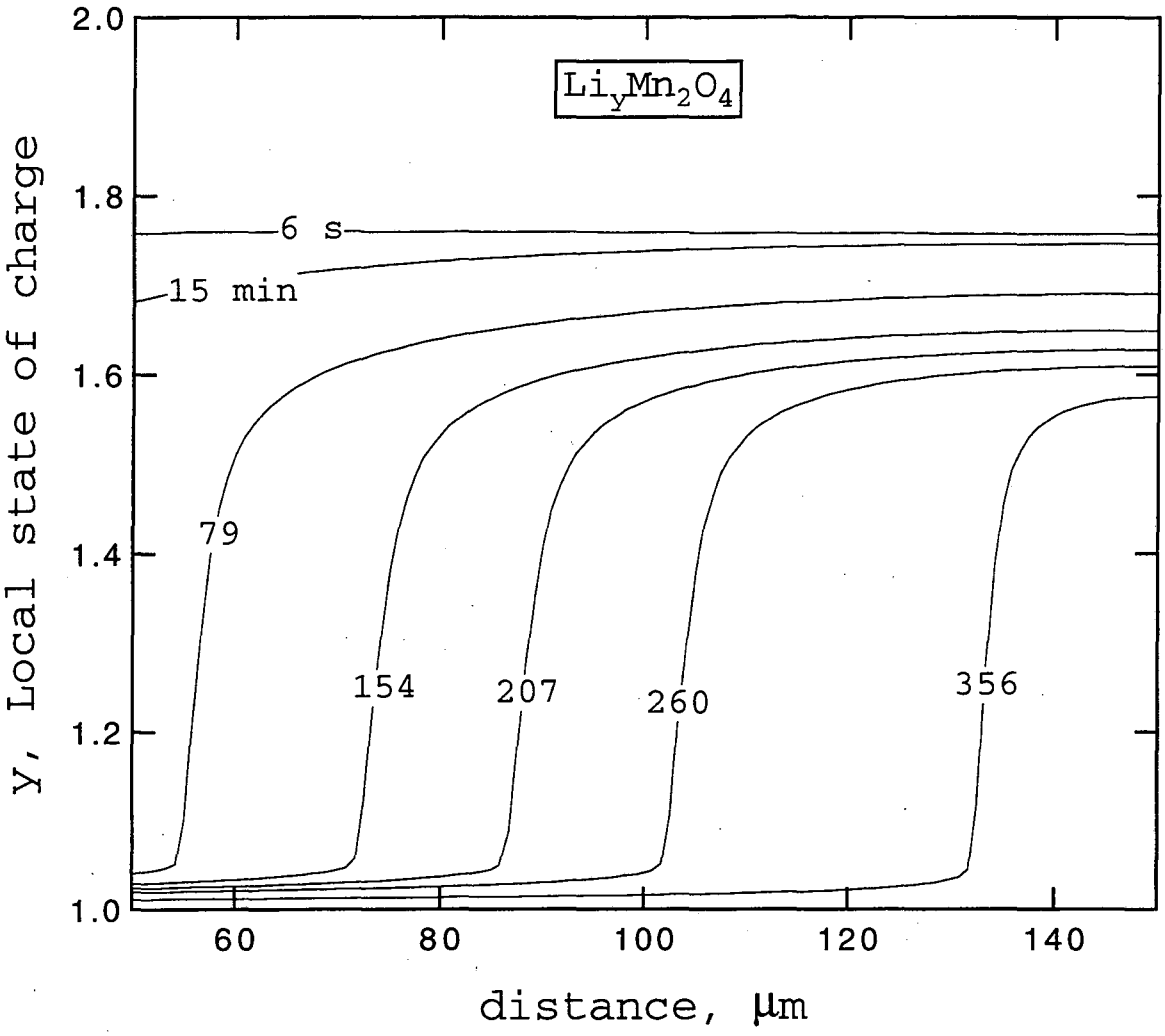

Figure 7. Local state of charge across the positive electrode during charging at I=-3.5 A/m^2. The curves correspond to section C on figure 2. Time since the beginning of charge is given as a parameter. Distance is measured from the negative electrode/separator interface.

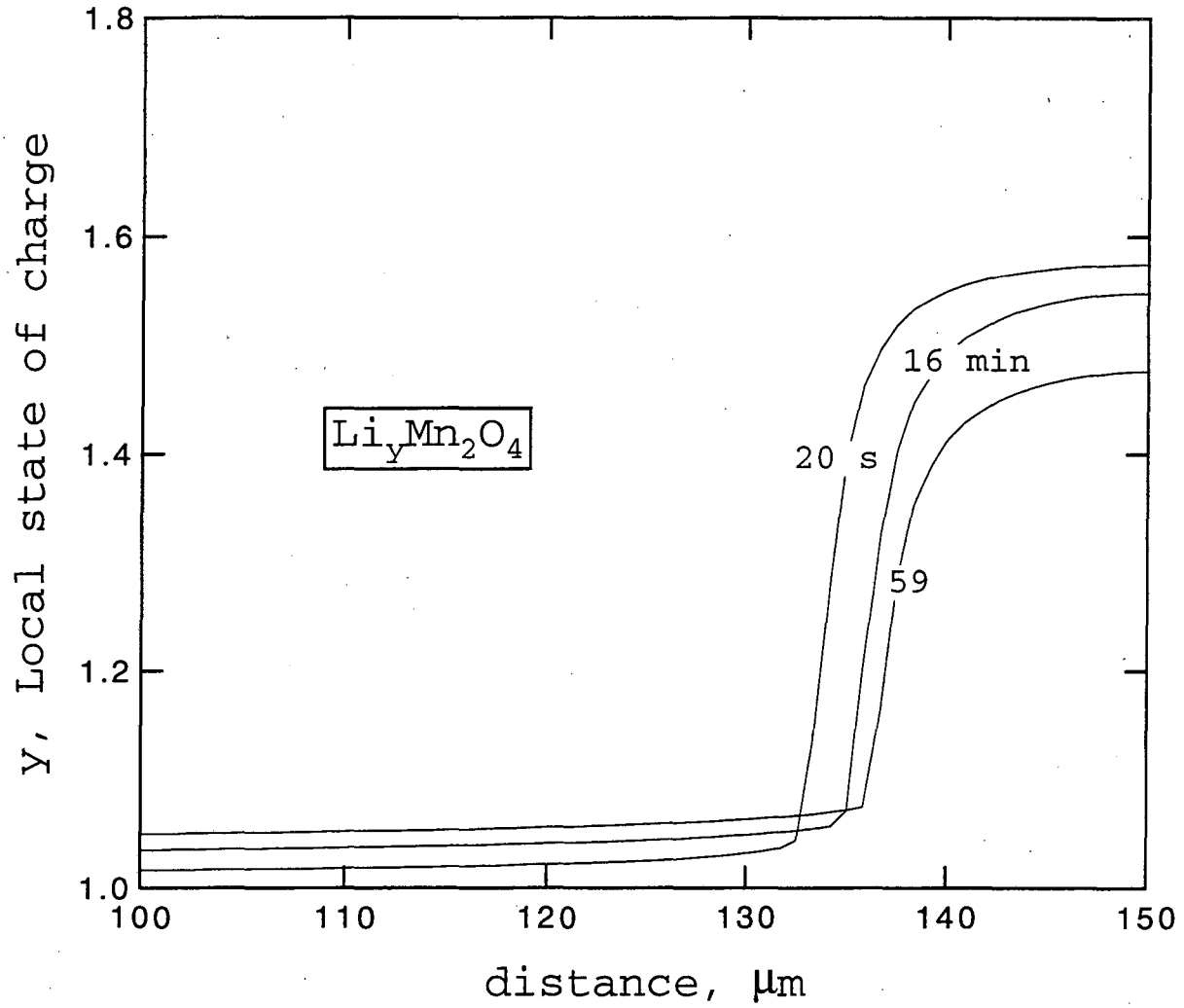

Figure 8. Local state of charge across the back half of the positive electrode during relaxation after a charge at I=-3.5 A/m^2. The curves correspond to section D on figure 2. Time since the beginning of the relaxation period is given as a parameter. Distance is measured from the negative electrode/separator interface.

Multiple cycles.—Having analyzed the full range of behavior of the system during discharge and charge with intermediate relaxation periods, we can now predict the consequences of these periods for extended cycling. First, we should realize that the conclusions here are strongly dependent on the particular insertion material studied, as we have seen that it is the shape of the open-circuit potential *vs*. state of charge that has the largest impact on the distribution of utilized material.

The cycling behavior is only slightly affected by the concentration gradients in the electrolyte, which may exist when relaxation times are not included. So, for example, charging curves (cell potential *vs*. state of charge) with and without a relaxation period after the previous discharge are insignificantly different if the local utilization is uniform. The major impact on multiple cycles comes from the equalization of the local state of charge. This, as we have seen, depends on the nonuniformity of the current distribution as the charge or discharge proceeds. The allowance of a relaxation time can correct for nonuniform-material utilizations by the spontaneous redistribution processes discussed earlier. However, this happens only if a significant driving force exists, meaning that the variation of state of charge must leave different parts of the electrode at different potentials.

The distributions of active material at the end of both a charge and a discharge are similar, in that the least accessible region, the back face of the electrode, is left either utilized or unutilized depending on the direction of current flow (compare short times on figures 5 and 8). This nonuniform utilization is desirable compared to an initially uniform distribution of active material on the subsequent cycle. This situation is depicted in figure 9, where the cell potential is simulated over three full cycles with one-hour relaxation periods between each half-cycle. On discharge from an initially uniform distribution of active material, the first cycle exhibits the largest overpotential at the cutoff point. The second and third cycles are "easier," *i.e*., the overpotential is smaller, because the charging periods leave the active material more charged at the front where it is more accessible on discharge. Notice that all three charging profiles are identical; this is because they all start

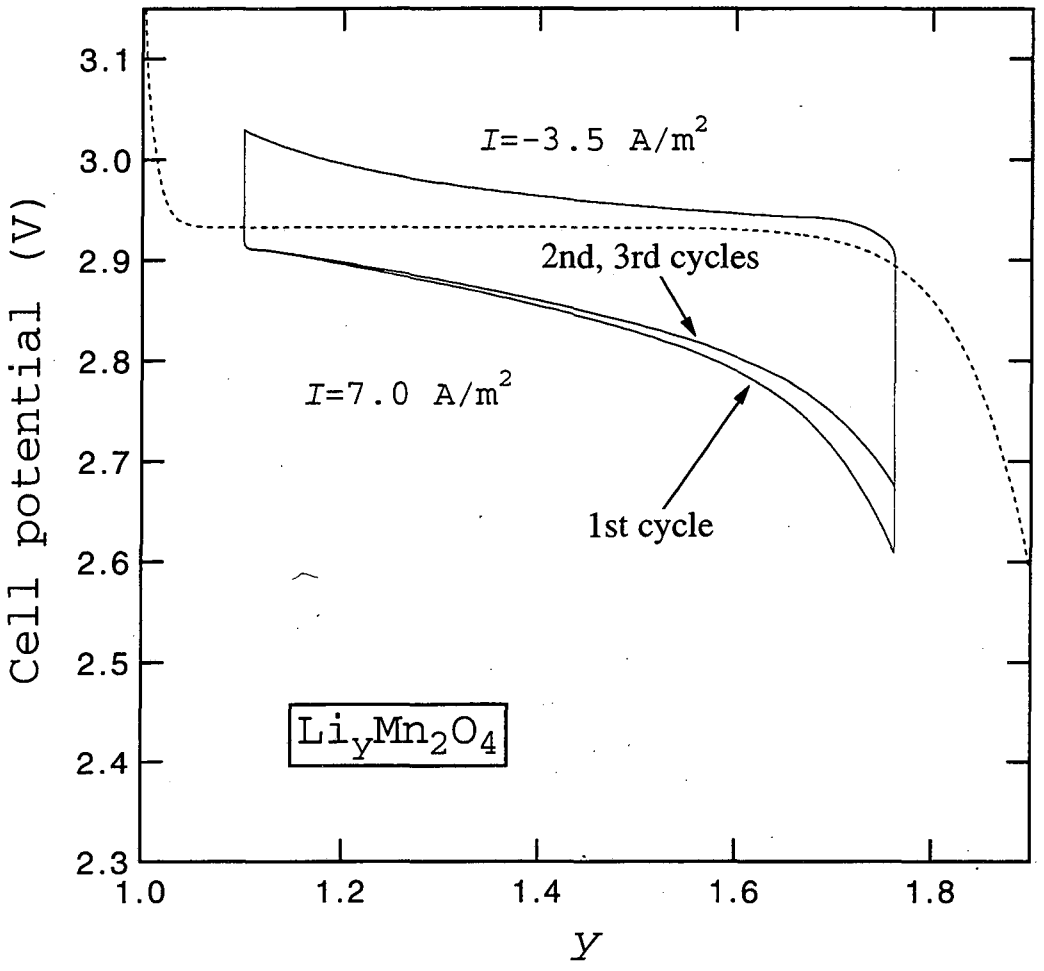

Figure 9. Cell potential *vs.* state of charge for the lithium/manganese dioxide system during three complete discharge/charge cycles at I=7.0 A/m^2 and I=-3.5 A/m^2, respectively. The dashed line is the open-circuit potential of the cell. There was a one-hour relaxation period between charge and discharge.

from the same point, a uniform distribution of material. Although not shown here, a cell that is discharged immediately following the charging process will have a slightly lower overpotential than a cell that is allowed to relax before discharging.

Peak power.—Here we consider the effect of a period of relaxation on the peak power attainable from the cell. As we have shown in earlier work, the peak power is greatly reduced at large depths of discharge[13] because the remaining active material becomes increasingly difficult to access. It is expected that a short period of cell relaxation would allow much of the performance to be recovered. The cell was discharged galvanostatically at the three-hour rate to 80% depth of discharge, and then the current was pulsed for 30 seconds. The value of the current was increased until the power went through a maximum. The mass of the cell includes active material, electrolyte, separator, and inert filler only. The power *vs.* current density, with the time of relaxation preceding the current pulse as a parameter, is shown in figure 10. Here we see that a relaxation period before pulsing the current greatly increases the available power. For this system, the cell is limited by the concentration of the electrolyte at the negative electrode exceeding c_{max}. The exchange-current density on the lithium foil electrode[1] approaches zero as the concentration approaches c_{max}. With the external current zero, the concentration gradients in the electrolyte relax quickly, and the peak power attainable increases. The maximum power at the initial conditions is about 221 W/m^2. Although a period of relaxation does not recover the performance at 0% depth of discharge, the peak power does increase substantially.

Dual lithium-ion-insertion cell.—Next, the Sony phone cell (Sony 20500 cell), described in the introduction, is simulated. The choice of parameters for the model, in particular the state of charge of each electrode, is discussed in appendix B. The battery has a capacity of about one A-h. Figure 11 shows the potential of the cell *vs.* capacity in A-h. The open-circuit potential of the cell is depicted by the dashed line. We simulated a high rate of discharge (86 A/m^2 or 1.9 A) for 16 minutes (labeled as A); at this rate the

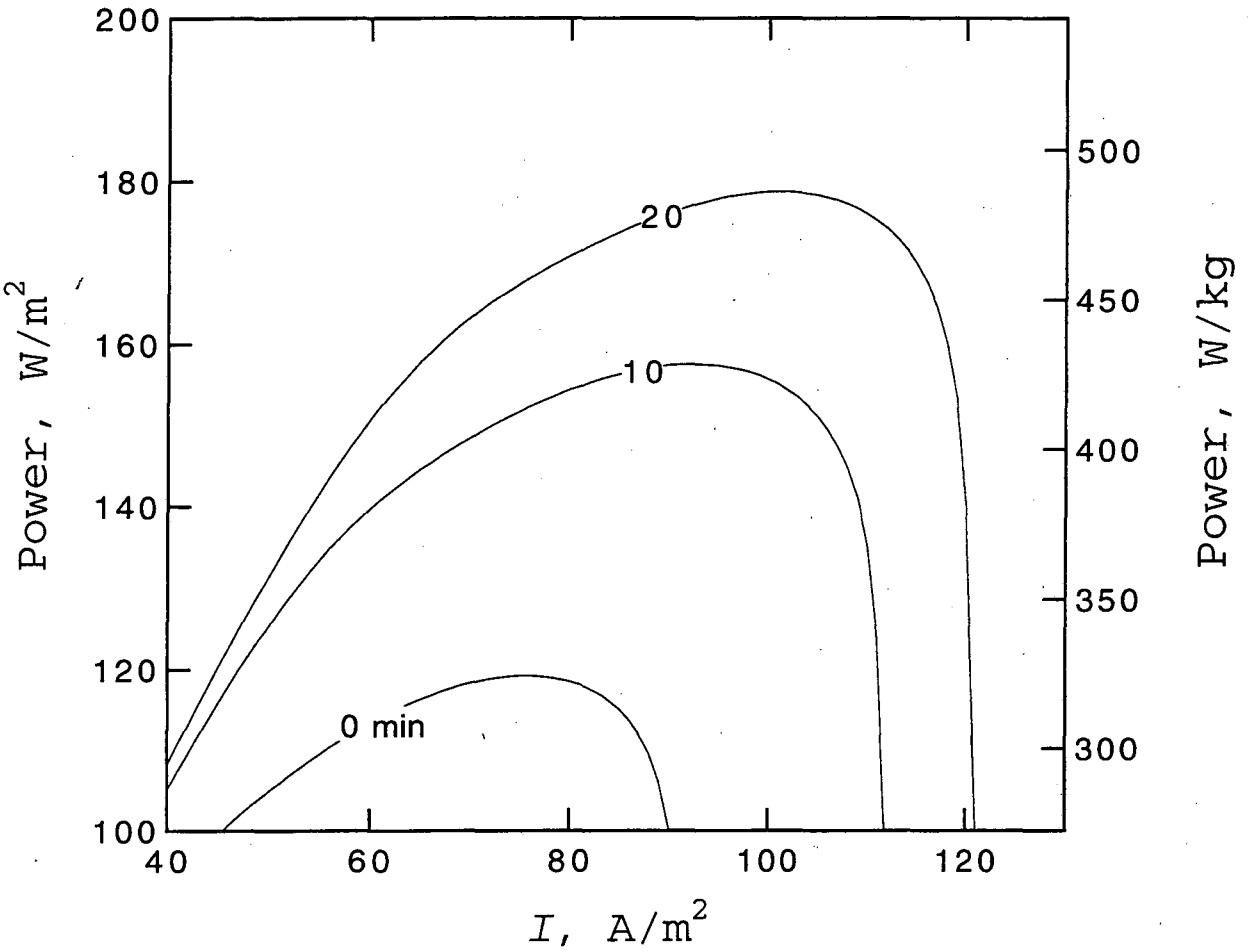

Figure 10. Power available for a thirty-second pulse of current. The cell was discharged at the three-hour rate to 80% depth of discharge prior to the current pulse. The relaxation time in minutes is a parameter. Maximum power for the fully charged cell is 221 W/m^2, and the mass of the cell is 0.3677 kg/m^2.

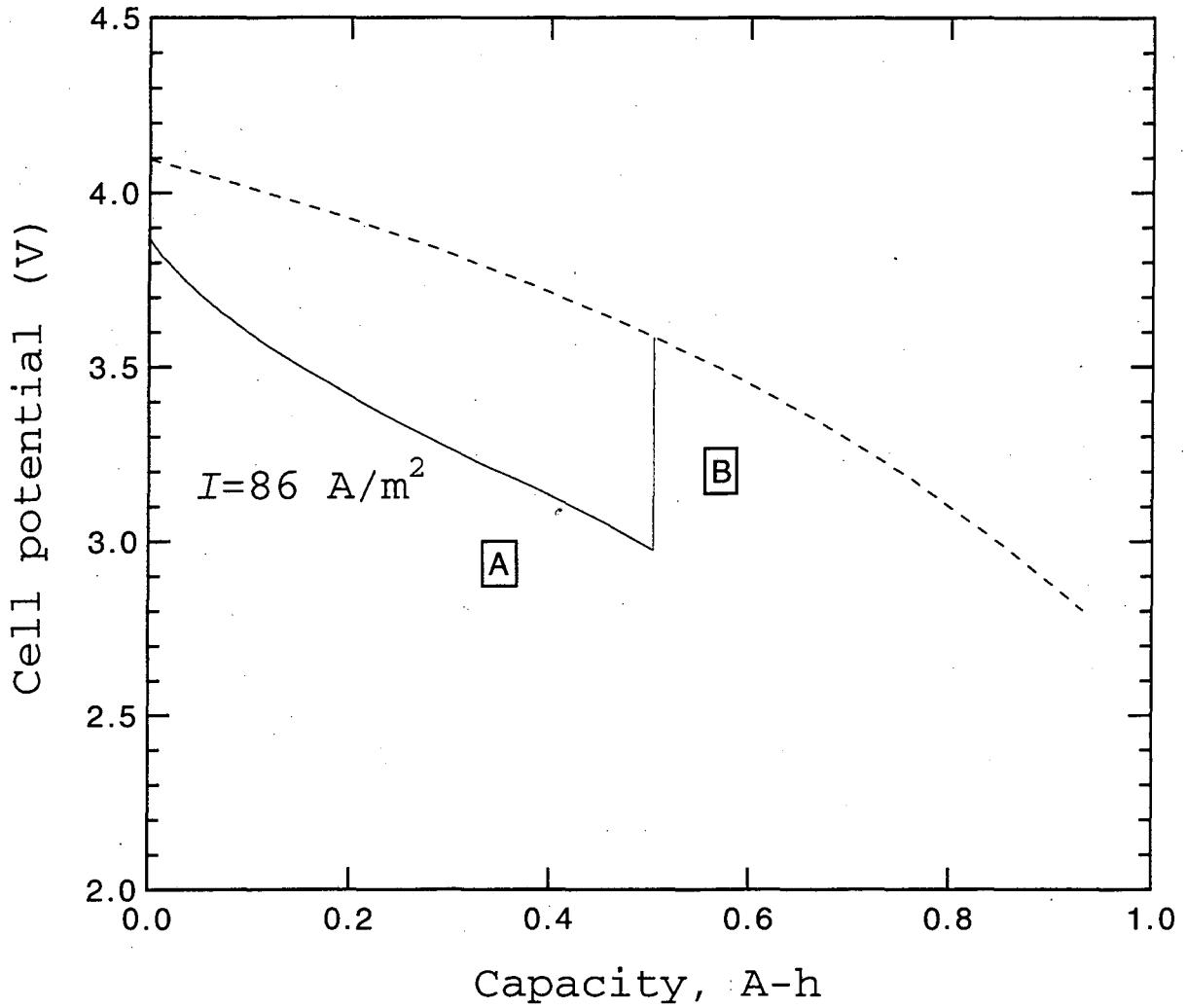

Figure 11. Simulation of a high-rate discharge of the Sony phone cell. The cell is discharged galvanostatically (A), followed by a relaxation period (B). The open-circuit potential is depicted by the dashed line.

maximum capacity is not attained before the potential drops below a prescribed cutoff value of 2.75 V (see figure 15). Our objective in choosing a high-rate discharge is to magnify the effects of gradients in concentration and nonuniform current distribution. The high current density also proved valuable in verifying the model with experimental data.

The cell is then allowed to relax for a one-hour period (labeled as B). Figure 12 plots the cell potential *vs.* time in minutes (time is measured from the beginning of the discharge). The potential initially jumps as the ohmic drop and surface overpotential in the cell change instantaneously. Next, there is a gradual climb of the cell potential as the concentration overpotential decreases while concentration gradients relax. This climb is perturbed by lithium redistribution processes that occur; hence the change in slope at about 25 minutes. The potential of the cell is close to the open-circuit value 20 minutes after current interruption.

The local state of charge within the cell is shown in figure 13. The negative (carbon) electrode is on the left, and the positive (cobalt dioxide) electrode on the right. For the negative electrode, lithium deinserts from the back of the electrode and inserts into the front (closest to the separator). The converse occurs in the positive electrode. These processes are both driven by the potential variations existing across the two electrodes, as discussed above for the manganese dioxide electrode. Both of these electrodes have sloping open-circuit potentials (see figure 18). The state of charge is completely uniform in both electrodes after about one hour.

Figure 14 shows the pore-wall flux into the particles over the same time period. The redistribution is faster in the carbon electrode. In particular, the negative electrode is almost completely relaxed after 9 minutes; the positive electrode does not reach a similar point until 31 minutes after current interruption. This difference arises because the local utilization is more nonuniform in the positive electrode, making the redistribution process there more substantial. The equalization occurs uniformly over the front and back of the negative electrode because of the highly sloping open-circuit potential for carbon. On the

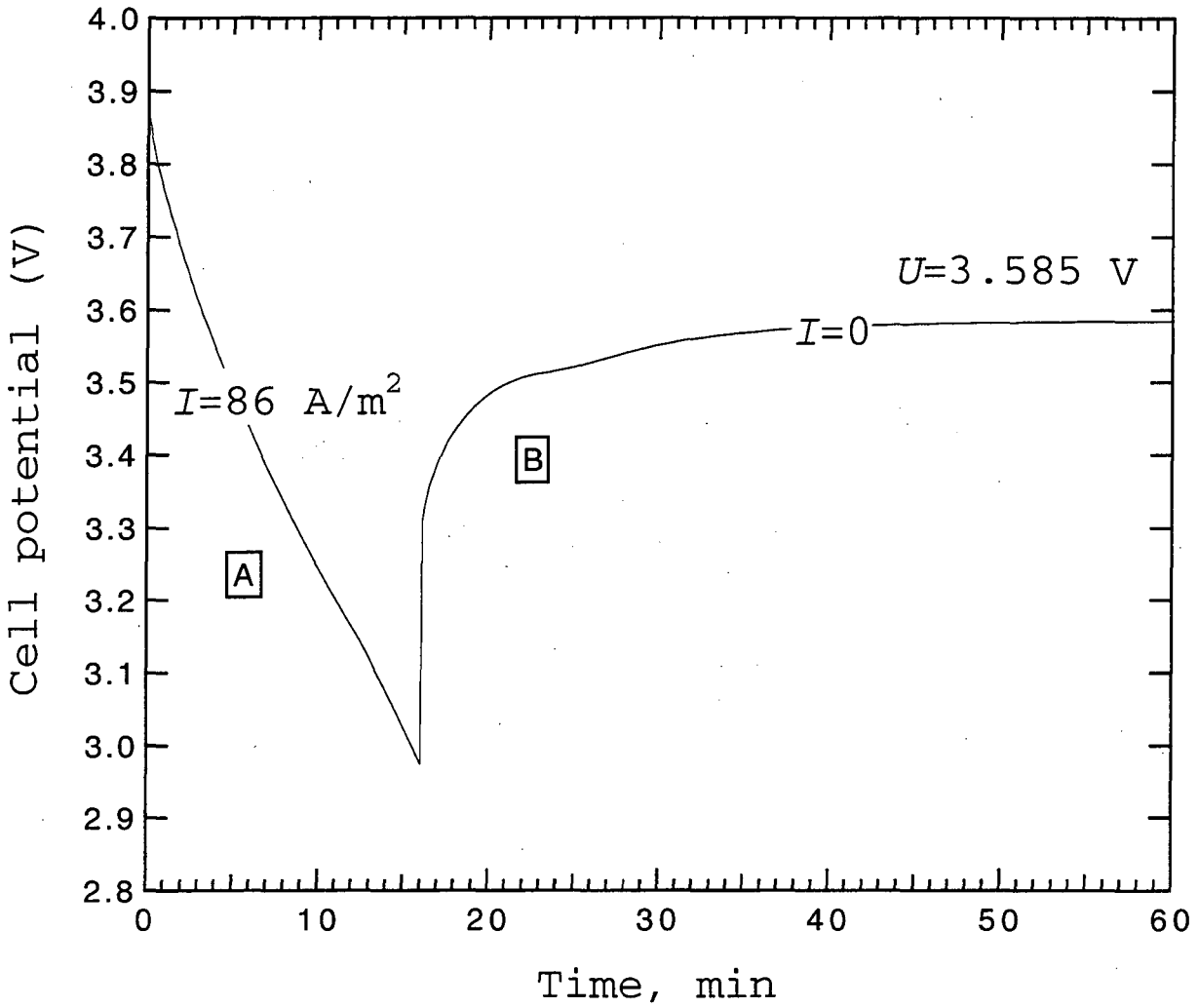

Figure 12. Cell potential *vs.* time for the Sony phone cell. The cell is discharged for 16 minutes before current interruption, and then the cell is allowed to relax.

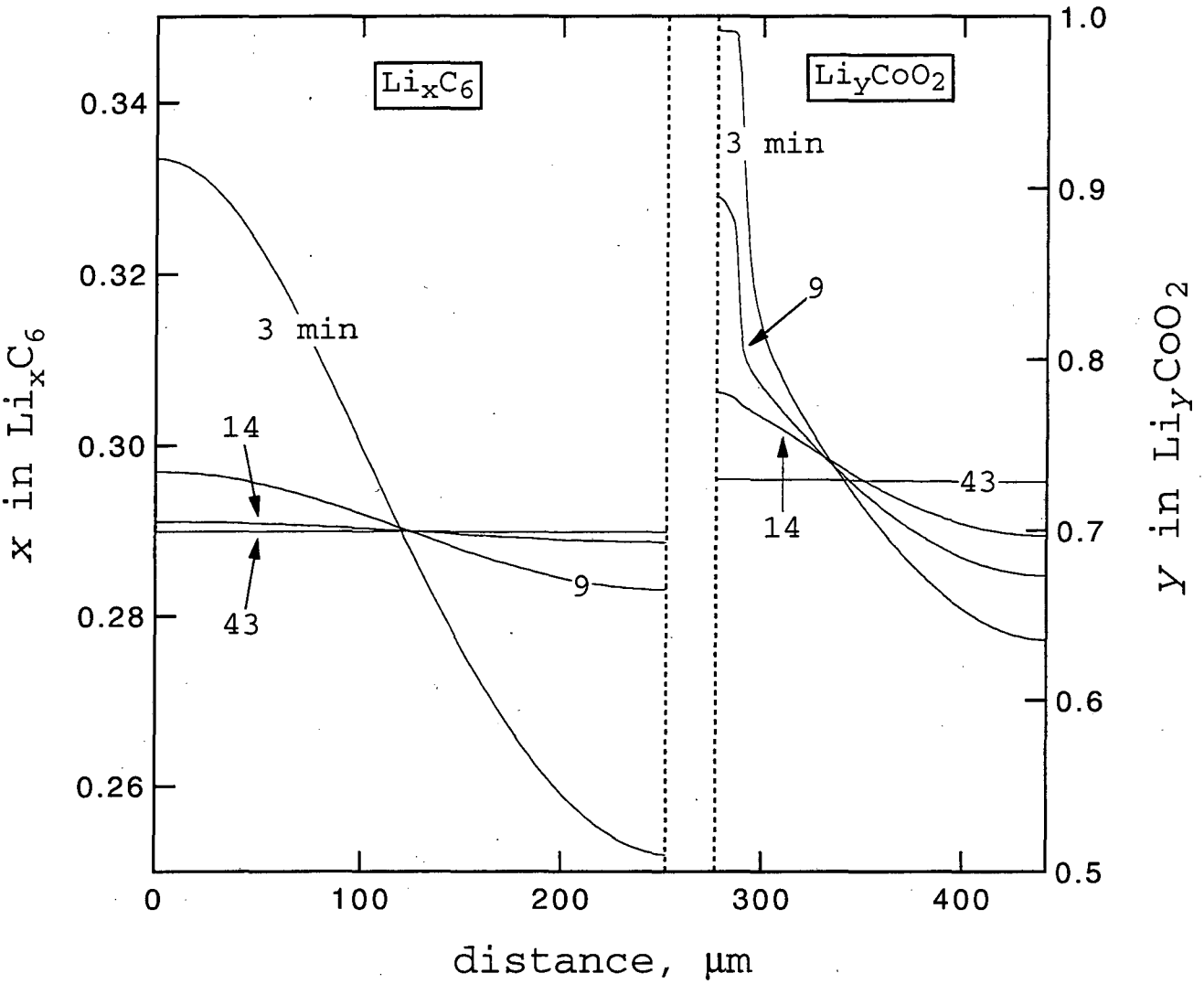

Figure 13. Local state of charge in the positive and negative electrodes during a relaxation period. The curves correspond to section B on figure 11. The dashed lines set off the separator region. Time is measure from the current interruption.

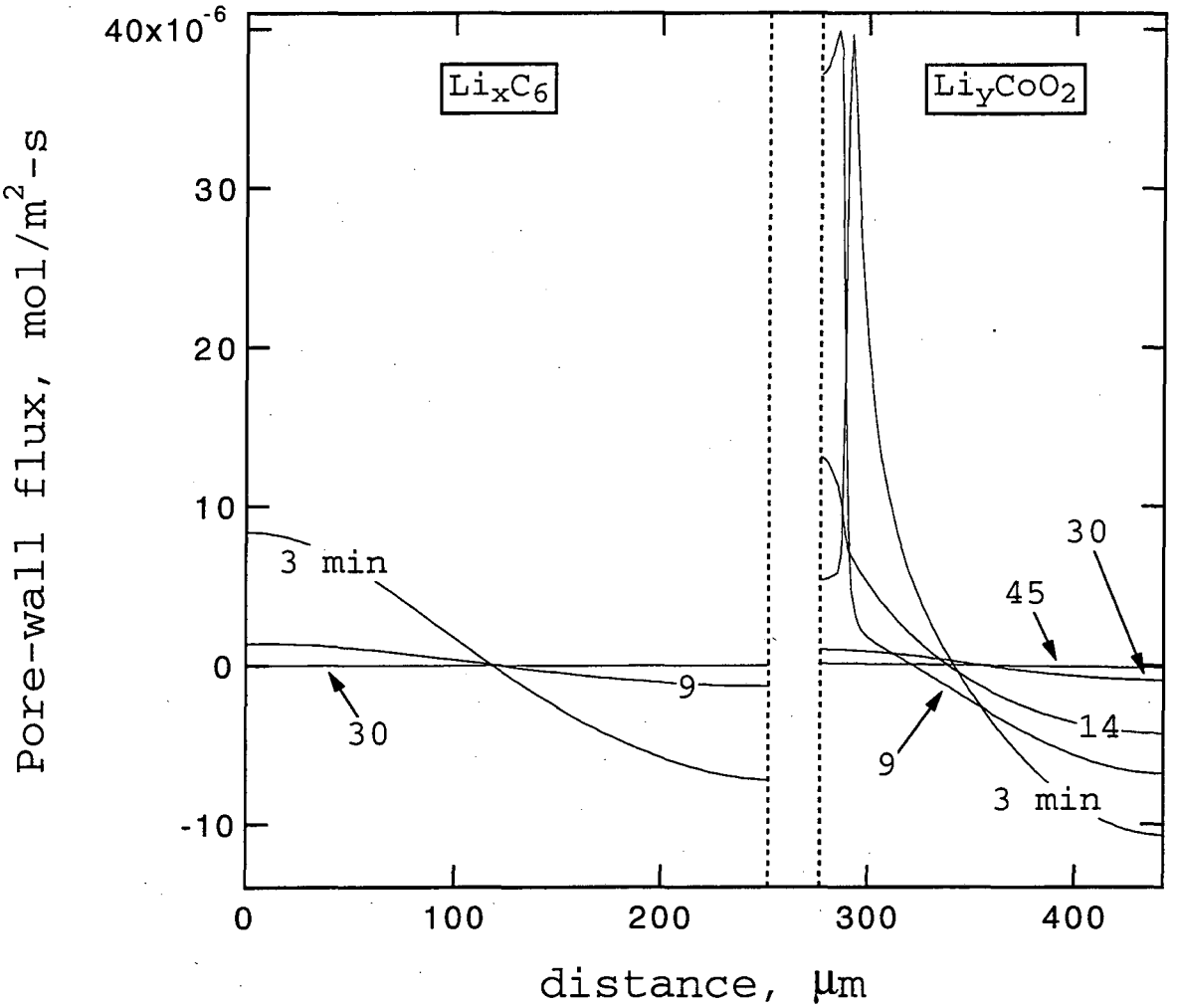

Figure 14. Pore-wall flux for the positive and negative electrodes during a relaxation period. The curves correspond to section B on figure 11. The dashed lines set off the separator region. Negative values correspond to insertion.

other hand, in the positive electrode a nonuniform deinsertion front moves toward the separator because the open-circuit potential of this region of the electrode is more nearly constant.

Potentiostatic charging.—Often galvanostatic charging of cells is not practical. The electrolyte may be unstable at high potentials, or unwanted side reactions may occur. In the Sony cell, for example, there is no overcharge mechanism, and it is necessary to keep the potential of the cell below about 4.1 V. We are now able to compare the results of simulations with experimental data for the Sony cell. The parameters selected for the model are discussed in appendix B. The same set of parameters was used in all of the simulations.

We simulated three galvanostatic discharges to a cut-off potential of 2.75 V. The cell is then charged galvanostatically to 4.1 V. Then, the potential is held constant until the number of coulombs passed brings the electrodes to the original states of charge. The potential of the cell predicted from the simulations is plotted in figure 15 for three charge/discharge cycles. The solid line is the open-circuit potential, the dashed lines are the simulations, and the markers correspond to experimental data. These data represent the fourth through the sixth cycles, where it is hoped that irreversible phenomena associated with the first few cycles will have abated. The agreement with the experimental data is good. As discussed in appendix B, the only truly adjustable parameter here is the electrolyte conductivity, and even this is fixed in form but not in magnitude. The comparison seems to be worst at the highest discharge rate, especially near the beginning of discharge. An initial sharp drop in the cell potential at high rates of discharge is a characteristic of the Sony cell. Our model does not accurately simulate this behavior.

During a potentiostatic charge, the current density decreases over time. This is shown in figure 16 for the second cycle of figure 15. The solid line is the simulation result, and the crosses are the experimental data. It is evident that the current density *vs.* time can be described with a single time constant for the potentiostatic charge. The time

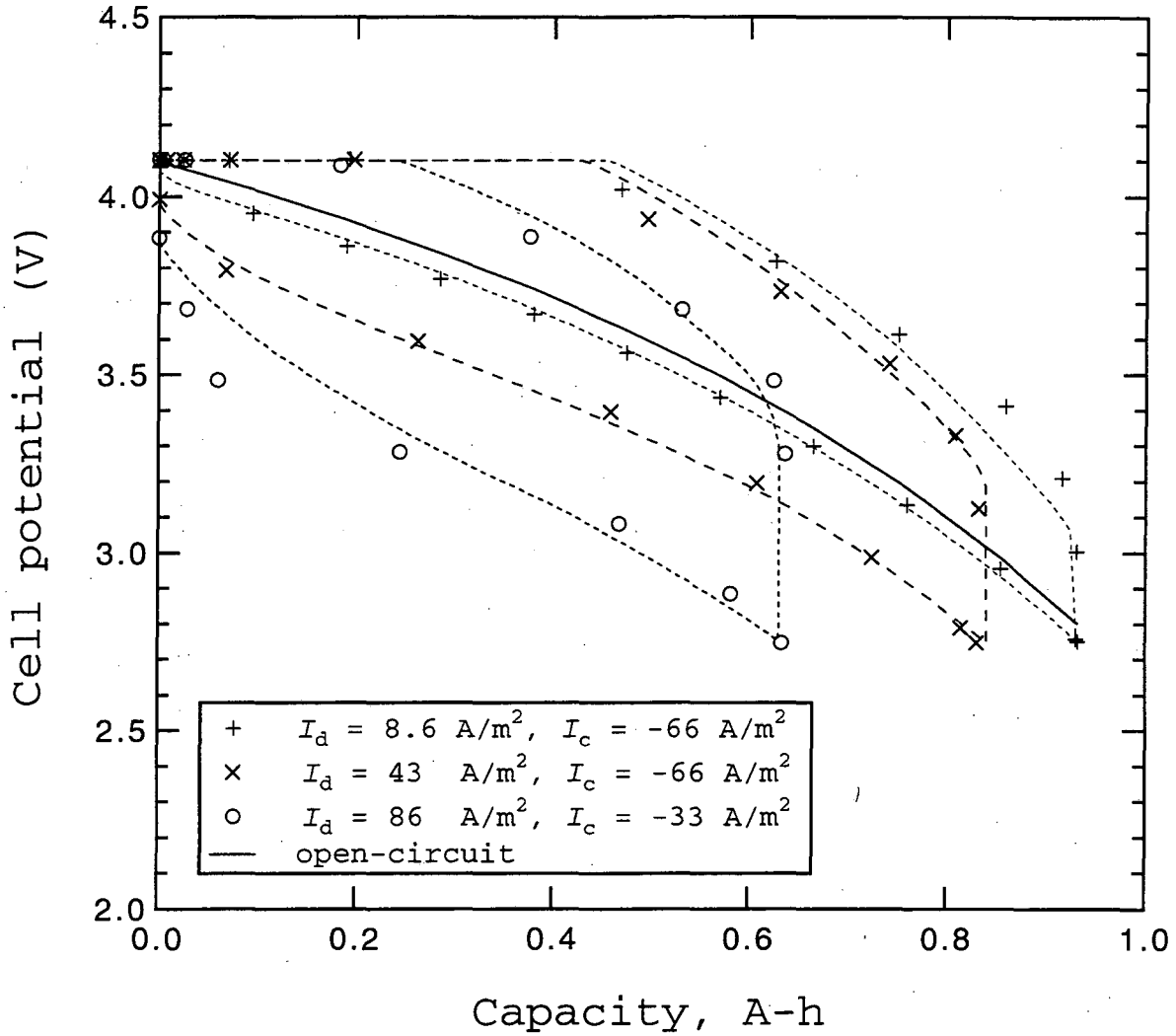

Figure 15. Simulation of the Sony phone cell. Experimental data are depicted by the markers, simulation results by the dashed lines, and the open-circuit potential by the solid line. The cell is discharged galvanostatically to 2.75 V and charged galvanostatically to 4.1 V (followed by a potentiostatic taper charge), with the discharge and charge rates given above.

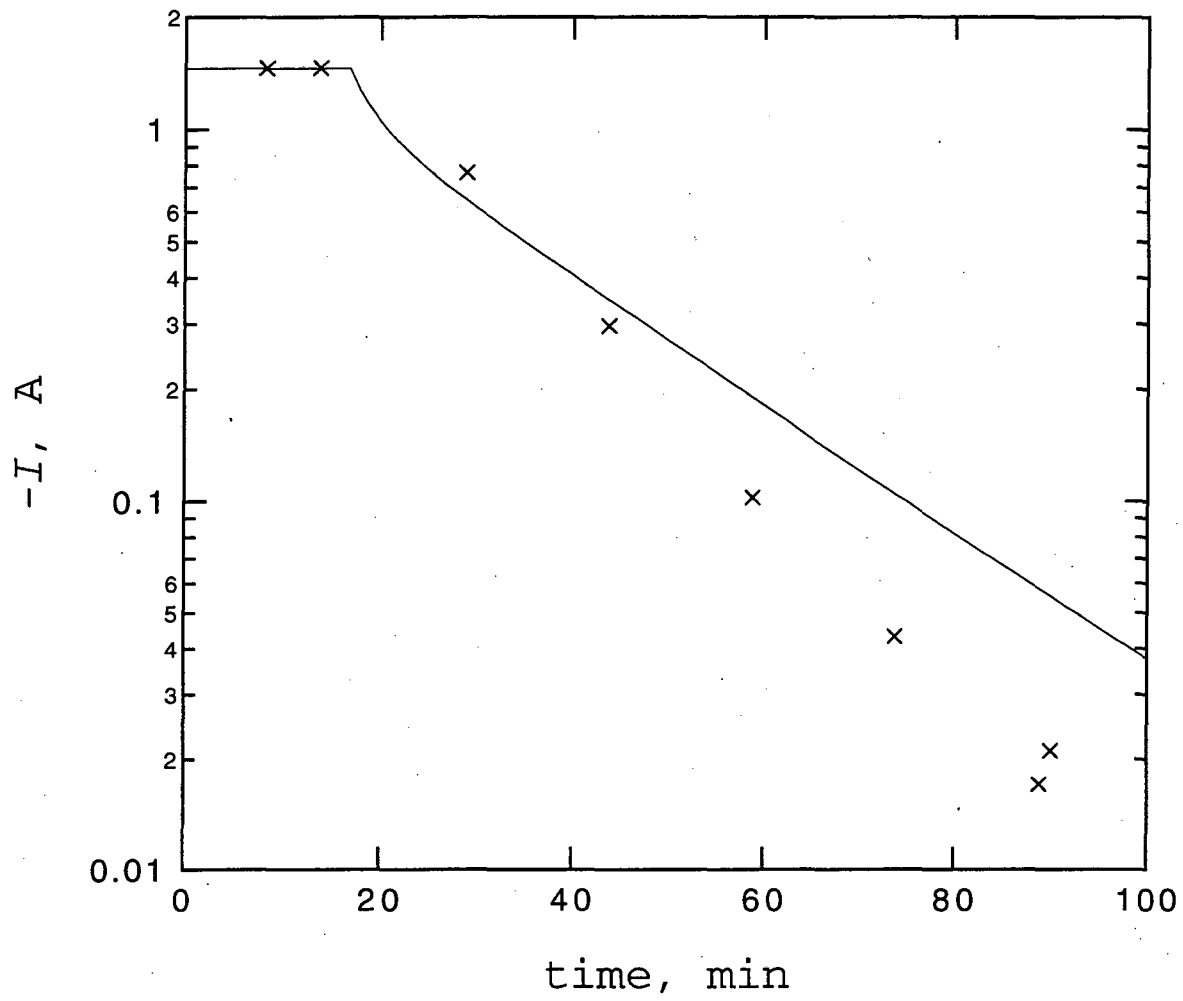

Figure 16. Current *vs.* time during potentiostatic charging for the Sony phone cell. Data are taken from the fourth cycle, following discharge at 0.95 A to 2.75 V. The cell was immediately charged galvanostatically to 4.1 V and then held at this potential. The solid line is the result of the simulation; the crosses are experimental data.

constant for potentiostatic charging of a composite electrode is approximated by $nFL^2(1-\varepsilon)/\kappa(dU/dc_s)$. The two slopes are roughly equal (17 and 25 min); but the time constant for the experimental data is smaller than that for the simulation results. This may suggest that the diffusion length is too large in the simulation (we increased the thickness of the negative electrode by about 20% to make the areas of the two electrodes equal).

Finally, in figure 17 we compare the capacity of the cell *vs.* current density. The cell was discharged galvanostatically to a cut-off potential of 2.75 V. The capacity is defined as the percentage of the A-h passed for the 0.2 A rate. The solid line is the simulation result, and the open circles are experimental values (for a fresh cell).[14] Although the agreement is not exceptional, the trend is evident. At high rates of discharge, ohmic losses are greater, and the electrolyte may be depleted in the back of the positive electrode. These polarizations limit the capacity of the cell. Again we find that the comparison with experimental data would be improved by decreasing the diffusion length used in the simulations.

Acknowledgments

This work was supported in part by the Assistant Secretary for Energy Efficiency and Renewable Energy, Office of Transportation Technologies, Electric and Hybrid Propulsion Division of the U. S. Department of Energy under Contract No. DE-AC03-76SF00098.

Appendix A: Summary of Model Equations

The model can be divided into the separator and composite electrode regions. In the solution phase of the composite electrode, the equations are

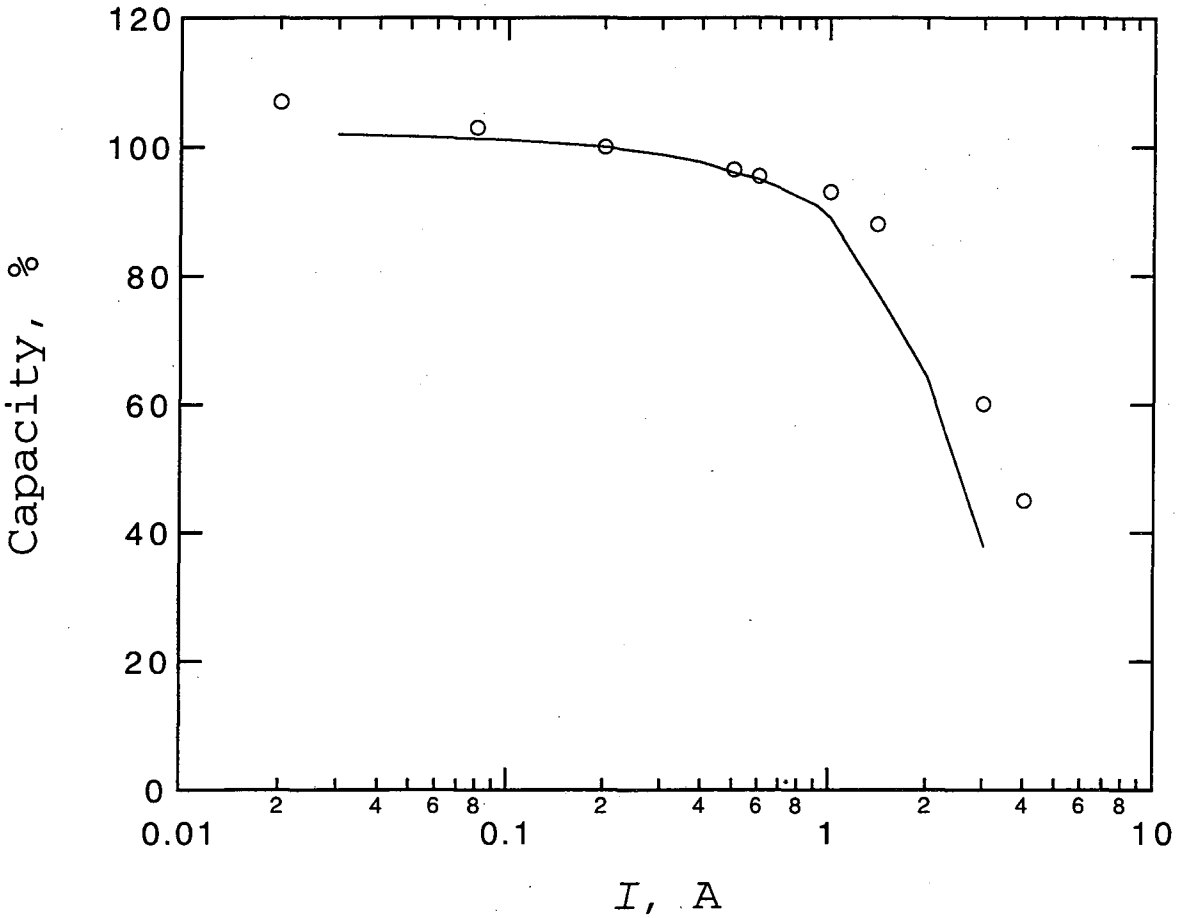

Figure 17. Capacity of the Sony cell *vs*. discharge current. Capacity is expressed as a percentage of the capacity in A-h, with the capacity at 0.2 A defined as 100%. Data from Sony corporation.[14] Solid line is the simulation result.

$$\varepsilon\frac{\partial c}{\partial t} = \nabla\cdot(\varepsilon D\nabla c) - \frac{\mathbf{i}_2\cdot\nabla t_+^0}{z_+\nu_+F} + \frac{aj_n\left(1-t_+^0\right)}{\nu_+}, \tag{A-1}$$

$$\mathbf{i}_2 = -\kappa\nabla\Phi_2 + \frac{\kappa RT}{F}\left(1+\frac{\partial\ln f_A}{\partial\ln c}\right)\left(1-t_+^0\right)\nabla\ln c, \tag{A-2}$$

$$aj_n = \frac{-s_i}{nF}\nabla\cdot\boldsymbol{i}_2. \tag{A-3}$$

In the solid phase of the composite electrodes

$$\boldsymbol{i}_1 = -\sigma\nabla\Phi_1, \tag{A-4}$$

$$\frac{\partial c_s}{\partial t} = D_s\left[\frac{\partial^2 c_s}{\partial r^2} + \frac{2}{r}\frac{\partial c_s}{\partial r}\right]. \tag{A-5}$$

These two phases are related through the boundary condition

$$j_n = -D_s\frac{\partial c_s}{\partial r} \text{ at } r = R_s, \tag{A-6}$$

as well as a Butler-Volmer kinetic expression.[1] In the separator region the first two equations apply with $j_n = 0$ These equations are linearized and solved simultaneously using the subroutine BAND.[9] We have two independent variables (x and t) and six dependent variables (c, Φ_2, c_s, $\boldsymbol{i}_2$, j_n, and Φ_1). The Crank-Nicolson implicit method was used to evaluate the time derivatives.

Appendix B: Transport and Thermodynamic Data Used in the Simulations

The potentials of the three electrodes were fit to analytic functions from data available in the literature. The open-circuit curves for carbon (petroleum coke)[15] and cobalt

dioxide[16] are shown in figure 18. The open-circuit curve for manganese dioxide (lower plateau) was given in figure 2.

The transport data used for lithium trifluoromethane sulfonate in polyethylene oxide include: conductivity,[12] transference number,[17] and diffusion coefficient.[16] The activity coefficient is not available with sufficient accuracy over a range of concentration.

Estimation of parameters for the Sony Cell.—Our model is one-dimensional and can only approximate the spirally wound Sony 20500 cell. Since the two electrodes must have the same area for the simulation, we increased the thickness of the negative electrode (keeping the capacity constant) to match the area for the positive electrode. Information for the mass of active material, porosity, *etc.*, were obtained from personal communications. Ohmic losses in the current collectors were neglected.

The capacities of the two electrodes were calculated based on the masses of active material in each electrode. We then assumed that the nominal capacity of the battery was 0.932 A-h (based on the experimental data), and estimated Δx, Δy, and z, the positive-to-negative capacity ratio. Since we did not have information on the state of charge of the individual electrodes, we estimated the initial values of x and y. From the open-circuit potentials of the two electrodes (figure 18) and their capacity ratio (z), we developed an expression for the open-circuit potential of the coupled electrodes *vs.* state of charge. The initial values of x^o and y^o were parameters. We did not have open-circuit data; consequently, we fit the experimental data taken at the lowest current density to our theoretical curve. With an estimate of x^o and y^o, we ran a numerical simulation at the current density in question. The difference in potential between the data and the simulation results was added to the data, representing a closer approximation to the open-circuit values. The values of x^o and y^o calculated from the iterative process are given in table 2 as the initial concentrations in the solid.

The electrolyte for this system is a combination of propylene carbonate and diethyl carbonate with a salt of lithium hexafluorophosphate (unknown concentration) and some

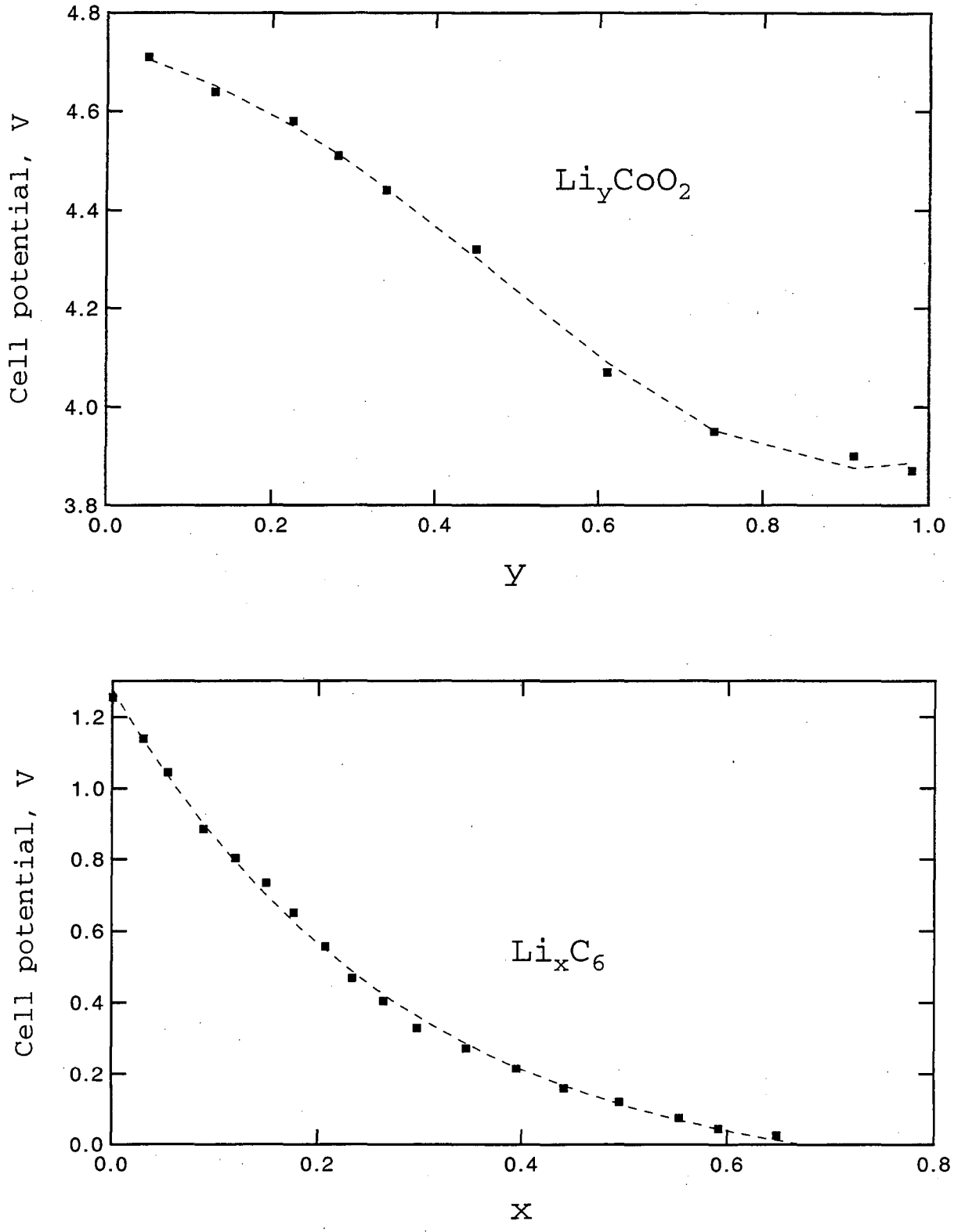

Figure 18. Open-circuit potential *vs.* state of charge for the carbon and cobalt dioxide materials. Data were obtained from the literature.

lithium carbonate. We did not have physical properties for this system, and so the following assumptions were made. First, we assumed that the dependence of conductivity is that given by Barthel *et al.*[18] (for $LiPF_6$ in propylene carbonate), but with the conductivity maximum as a parameter. The diffusion coefficient was assumed to be 2.58×10^{-10} m^2/s, a value reported for lithium perchlorate in propylene carbonate,[19] and the transference number was assumed to be 0.2. The conductivity maximum was adjusted to match the simulation results with the experimental data shown in figure 15. Hence, the conductivity is represented by

$$c^{1.093}\,5.846\times10^{-4}\exp\left\{0.04\left(\frac{c}{1204}-0.897\right)^2-\frac{c}{944}+1.093\right\}. \qquad \text{(B-1)}$$

The separator was assumed to have a porosity of 0.38, typical of the porosity of Celgard® used for lithium cells. All of the simulations of the dual insertion cell used the same set of parameters.

List of Symbols

a	specific interfacial area, m^2/m^3
c	concentration of electrolyte, mol/m^3
c_i	concentration of species i, mol/m^3
c_s	concentration of lithium in solid phase, mol/m^3
C	double-layer capacitance, F/m^2
D,D_s	diffusion coefficient of electrolyte and of lithium in the solid matrix, m^2/s
f_A	activity coefficient of the salt
F	Faraday's constant, 96,487 C/eq
i	current density, A/m^2
i_o	exchange-current density, A/m^2

I	superficial current density, A/m^2
j_n	pore-wall flux across interface, mol/m^2-s
L	thickness of the cell, m
n	number of electrons transferred in electrode reaction
r	radial distance within a particle of active material, m
R	universal gas constant, 8.314 J/mol-K
R_s	radius of electrode material, m
s_i	stoichiometric coefficient of species i in electrode reaction
S_s,S_e	dimensionless ratios defined in equations 1 and 2
t	time, s
t_i	transference number of species i
T	temperature, K
U	open-circuit potential, V
V	cell potential, V
x	stoichiometric coefficient for negative electrode
y	stoichiometric coefficient for positive electrode
z	capacity ratio of positive to negative electrode
z_i	charge number of species i
δ_s	thickness of separator, m
δ_+	thickness of positive electrode, m
δ_-	thickness of negative electrode, m
ε	porosity
κ	electrical conductivity of the electrolyte, S/m
μ_i	electrochemical potential, J/mol
ν_+,ν_-	number of cations and anions into which a mole of electrolyte dissociates
σ	electrical conductivity of solid matrix, S/m
Φ	electrical potential, V

Subscripts

e	electrolyte
f	filler
s	solid phase or separator
t	concentration in insertion material corresponding to y=1
1	solid matrix
2	solution phase
+	positive electrode
-	negative electrode

Superscripts

0	solvent or initial condition
θ	standard cell potential

References

1. M. Doyle, T. F. Fuller, and J. Newman, "Modeling of the Galvanostatic Charge and Discharge of the Lithium/polymer/insertion Cell," *J. Electrochem. Soc.*, **140**, 1526 (1993).

2. T. F. Fuller, M. Doyle, and J. Newman, "Simulation and Optimization of the Dual Lithium Ion Insertion Cell," submitted to *J. Electrochem. Soc.*, May, 1993.

3. Sony's Lithium Manganese Rechargeable Battery (AA Size), *JEC Press, Inc.*, p. 26 (February, 1988).

4 . R. Pollard and J. Newman, "Mathematical Modeling of the Lithium-Aluminum, Iron Sulfide Battery, *J. Electrochem. Soc.*, **128**, 503-507 (1981).

5. D. Guyomard and J. M. Tarascon, "Li Metal-Free Rechargeable $LiMn_2O_4$/Carbon Cells: Their Understanding and Optimization," *J. Electrochem. Soc.*, **139**, 937-948 (1992).

6. C. A. C. Sequeira and A. Hooper, "The Study of Lithium Electrode Reversibility against PEO-$LiCF_3SO_3$ Polymeric Electrolytes," *Solid State Ionics*, **9&10**, 1131 (1983).

7 . S. Kikkawa, S. Miyazaki, and M. Koizumi, "Electrochemical Aspects of the Deintercalation of Layered AMO_2 Compounds," *J. Power Sources*, **14**, 231-234 (1985).

8. M. G. Thomas, P. G. Bruce, and J. B. Goodenough, "AC Impedance of the $Li_{(1-x)}CoO_2$ Electrode, *Solid State Ionics*, **18&19**, 794 (1986).

9 J. Newman, *Electrochemical Systems*, p. 472, Prentice Hall, Englewood Cliffs, N. J. (1991).

10. A. A. Mason, "Modeling and Optimization of Li-Alloy/Metal-Sulfide Molten Salt Batteries," M.S. Thesis, University of California, Berkeley (1988).

11. W. J. Macklin, R. J. Neat, and R. J. Powell, "Performance of Lithium-Manganese Oxide Spinel Electrodes in a Lithium Polymer Electrolyte Cell," *J. Power Sources*, **34**, 39 (1991).

12. C. D. Robitaille and D. Fauteux, "Phase Diagrams and Conductivity Characterization of Some PEO-LiX Electrolytes," *J. Electrochem. Soc.*, **133**, 315 (1986).

13. M. Doyle, T. F. Fuller, and J. Newman, "The Importance of the Lithium Ion Transference Number in Lithium/Polymer Cells," submitted to *Electrochim. Acta*, July 1993.

14. K. Ozawa and M. Yokokawa, "Cycle Performance of Lithium Ion Rechargeable Battery," Tenth International Seminar of Primary and Secondary Battery Technology and Applications, Deerfield, Florida, March, 1993.

15. R. Fong, U. von Sacken, and J. R. Dahn, "Studies of Lithium Intercalation into Carbon Using Nonaqueous Electrochemical Cells," *J. Electrochem. Soc.*, **137**, 2009 (1990).

16. K. Mizushima, P. C. Jones, P. J. Wiseman, and J. B. Goodenough, "Li_xCoO_2 ($0<x<1$); A New Cathode Material for Batteries of High Energy," *S. S. Ionics*, **3&4**, 171 (1981).

17. A. Bouridah, F. Dalard, D. Deroo, and M. B. Armand, "Potentiometric Measurements of Ionic Transport Parameters in Poly(ethylene oxide)-LiX Electrolytes," *J. Appl. Electrochem.*, **17**, 625 (1987).

18. J. Barthel, H. J. Gores, and G. Schmeer, "The Temperature Dependence of the Properties of Electrolyte Solutions. III. Conductance of Various Salts at High Concentrations in Propylene Carbonate at Temperatures from -45°C to +25°C," *Ber. Bunsenges. Phys. Chem.*, **83**, 911-920 (1979).

19. K. West, T. Jacobsen, and S. Atlung, "Modeling of Porous Insertion Electrodes with Liquid Electrolytes," *J. Electrochem. Soc.*, **129**, 1480 (1982).

LAWRENCE BERKELEY LABORATORY
UNIVERSITY OF CALIFORNIA
TECHNICAL INFORMATION DEPARTMENT
BERKELEY, CALIFORNIA 94720